Diagnosing Keratoconus Using VHF Digital Ultrasound Epithelial Thickness Profiles

13

Dan Z. Reinstein, Timothy J. Archer, Marine Gobbe, Raksha Urs, and Ronald H. Silverman

13.1 Introduction

Keratoconus is a progressive corneal dystrophy which manifests as corneal thinning and formation of a cone-shaped protrusion. Because laser refractive surgery may lead to accelerated postoperative ectasia in patients with keratoconus [1, 2], the accurate detection of early keratoconus is a major safety concern. The prevalence of keratoconus in the Caucasian population is approximately 1/2000 [3]. The incidence of undiagnosed keratoconus presenting to refractive surgery clinics tends to be much higher than this, as keratoconics develop astigmatism that is more difficult to correct by contact lenses or glasses, leading them to consider refractive surgery [4]. The challenge for keratoconus screening is to have high sensitivity, but for this to be combined with high specificity to minimize the number of atypical normal patients who are denied surgery.

As has been described in other chapters, there have been significant efforts made to develop methods for screening of early keratoconus over the last 30 years. In 1984, Klyce [5] introduced color-coded maps derived from computerized front surface placido topography, which have made the diagnosis of keratoconus easier, as patterns including inferior steepening, asymmetric bow-tie and skew bow-tie typical of keratoconus can be seen early in the progression of the disease [6, 7]. Placido-based instruments producing maps of anterior surface topography and curvature became available by the early 1990s and their use in keratoconus screening demonstrated [7–16]. Characterization of corneal thickness and topography of both corneal surfaces using scanning-slit tomography was introduced commercially in the mid-1990s by the Orbscan scanning slit system (Bausch & Lomb, Rochester, NY) [17–19] and later by the Pentacam rotating Scheimpflug-based system (Oculus Optikgeräte, Wetzlar, Germany) [20, 21] and other tomogra-

D.Z. Reinstein, M.D., M.A.(Cantab), F.R.C.S.C., F.R.C. Ophth (✉)
London Vision Clinic, London, UK

Columbia University Medical Center, New York, NY, USA

Centre Hospitalier National d'Ophtalmologie, Paris, France

School of Biomedical Sciences, University of Ulster, Coleraine, UK
e-mail: dzr@londonvisionclinic.com

T.J. Archer, M.A.(Oxon), DipCompSci(Cantab)
M. Gobbe, M.S.T.(Optom), Ph.D.
London Vision Clinic, London, UK
e-mail: tim@londonvisionclinic.com; marine@londonvisionclinic.com

R.Urs, Ph.D.
Department of Ophthalmology, Columbia University Medical Center, New York, NY

R. H. Silverman, Ph.D.
Department of Ophthalmology, Columbia University Medical Center, New York, NY

F.L. Lizzi Center for Biomedical Engineering, Riverside Research, New York, NY

J.L. Alió (ed.), *Keratoconus*, Essentials in Ophthalmology, DOI 10.1007/978-3-319-43881-8_13

phy scanners. Wavefront assessment [22] and the Ocular Response Analyzer (Reichert, Depew, NY) [23] have been employed as a means for detecting early keratoconus.

Topographic and tomographic evaluation has evolved from qualitative observation [7] to quantitative measurements, and many parameters have been described to aid the differentiation of normal from keratoconus eyes [7–16]. Several statistical and machine-based or computerized learning models have been employed for keratoconus detection, and automated systems for screening based on front and back surface topography and whole corneal tomography and pachymetric profile have been developed [20, 24–31].

Although these approaches have improved the effectiveness of keratoconus screening, there still remain equivocal cases where a confident diagnosis cannot be made and undiagnosed keratoconus remains probably the leading cause of corneal ectasia after LASIK [32–44]. The addition of quantitative parameters that are independent of those now obtained by topographic and tomographic analysis could potentially improve screening.

The corneal epithelial and stromal thickness profiles may represent such an independent parameter and will be the focus of this chapter. As will be described later, the corneal epithelium has the ability to alter its thickness profile to re-establish a smooth, symmetrical optical outer corneal surface and either partially or totally mask the presence of an irregular stromal surface from front surface topography [45, 46]. Therefore, the epithelial thickness profile would be expected to follow a distinctive pattern in keratoconus to partially compensate for the cone.

To formally distinguish abnormal from normal epithelial thickness profiles, we set out to study a population of normal eyes to define the normal epithelial thickness profile. In parallel, we also set out to study the epithelial thickness profile in a population of keratoconic eyes to describe epithelial changes with keratoconus. Knowing the epithelial thickness profile in each population, we aimed to qualitatively assess the differences to be able to discriminate between the two populations. Any departure from a normal epithelial thickness profile might be used as a very sensitive indicator of stromal surface irregularity and therefore as a tool to detect early keratoconus.

13.2 VHF Digital Ultrasound Arc Scanning

All of the epithelial thickness data that is described in this chapter was obtained using the Artemis very high-frequency digital ultrasound arc scanner (ArcScan Inc., Golden, CO), which has been previously described in detail [47–49]. Briefly, Artemis VHF digital ultrasound is carried out using an ultrasonic standoff medium. The patient sits and positions the chin and forehead into a headrest while placing the eye in a soft rimmed eyecup. Warm sterile normal saline (33 °C) is filled into the darkened scanning chamber. The patient fixates on a narrowly focused aiming beam which is coaxial with the infrared camera, the corneal vertex and the centre of rotation of the scanning system. The technician adjusts the centre of rotation of the system until it is coaxial with the corneal vertex. In this manner, the position of each scan plane is maintained about a single point on the cornea and corneal mapping is therefore centred on the corneal vertex. The Artemis VHF digital ultrasound uses a broadband 50 MHz VHF ultrasound transducer (bandwidth approximately 10–60 MHz) which is swept by a reverse arc high-precision mechanism to acquire B-scans as arcs that follow the surface contour of anterior or posterior segment structures of interest. Performing a 3D scan set with the Artemis 1 takes approximately 2–3 min per each eye.

Using VHF digital ultrasound, interfaces between tissues are detected at the location of the maximum change in acoustic impedance (the product of the density and the speed of sound). It was first demonstrated in 1993 that acoustic interfaces being detected in the cornea were located spatially at the epithelial surface and at the interface between epithelial cells and the

anterior surface of Bowman's layer [50]. This indicated that stromal thickness measurement with VHF digital ultrasound includes Bowman's layer. The posterior boundary of the stroma with VHF digital ultrasound is located at the interface between the endothelium and the aqueous as this is the location of the maximum change in acoustic impedance. This indicated that stromal thickness measurement with VHF digital ultrasound includes Descemet's and the endothelium.

13.2.1 Three-Dimensional Epithelial Pachymetric Topography

For three-dimensional scan sets, the scan sequence consisted of four meridional B-scans at 45° intervals. Each scan sweep takes about 0.25 s and consisted of 128 scan lines or pulse echo vectors. Ultrasound data are digitized and stored. The digitized ultrasound data are then transformed using patented Cornell University digital signal processing technology which includes auto-correlation of back surface curvatures to centre and align the meridional scans. A speed of sound constant of 1640 m/s was used. A linear polar–radial interpolation function is used to interpolate between scan meridians to produce a Cartesian matrix over a 10 mm diameter in 0.1 mm steps.

13.3 Epithelial Thickness Profile in Normal Eyes

We set out to characterize the in vivo epithelial thickness profile in a population of normal eyes with no ocular pathology other than refractive error. We obtained the epithelial thickness profile across the central 10 mm diameter of the cornea for 110 normal eyes of 56 patients and averaged the data in the population. Epithelial thickness values for left eyes were reflected in the vertical axis and superimposed onto the right eye values so that nasal/temporal characteristics could be combined [49].

The average epithelial thickness map revealed that the epithelium was not a layer of homogeneous thickness as had previously been thought but followed a very distinct pattern (Fig. 13.1a); on average the epithelium was 5.7 μm thicker inferiorly than superiorly, and 1.2 μm thicker temporally than nasally. The pattern of thicker epithelium inferiorly than superiorly and thicker epithelium nasally than temporally was consistent across a majority of eyes in the population sampled. The average central epithelial thickness was 53.4 μm and the standard deviation was only 4.6 μm [49]. This indicated that there was little variation in central epithelial thickness in the population. The thinnest epithelial point within

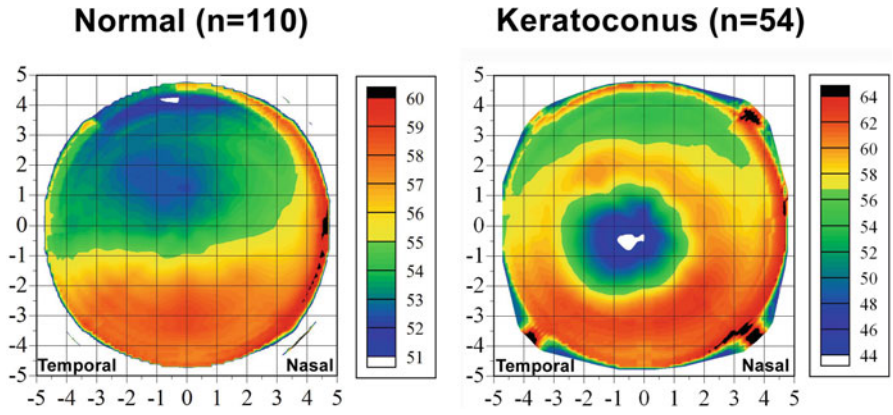

Fig. 13.1 Mean epithelial thickness profile for a population of 110 normal eyes and a population of 54 keratoconic eyes. The epithelial thickness profiles for all eyes in each population were averaged using mirrored left eye symmetry. The colour scale represents epithelial thickness in microns. A Cartesian 1-mm grid is superimposed with the origin at the corneal vertex. *Reprinted with permission from SLACK Incorporated*: *Reinstein, DZ., Archer, T., Gobbe M. (2009). "Corneal Epithelial Thickness Profile in the Diagnosis of Keratoconus." Journal or Refractive Surgery, 25, 604–610*

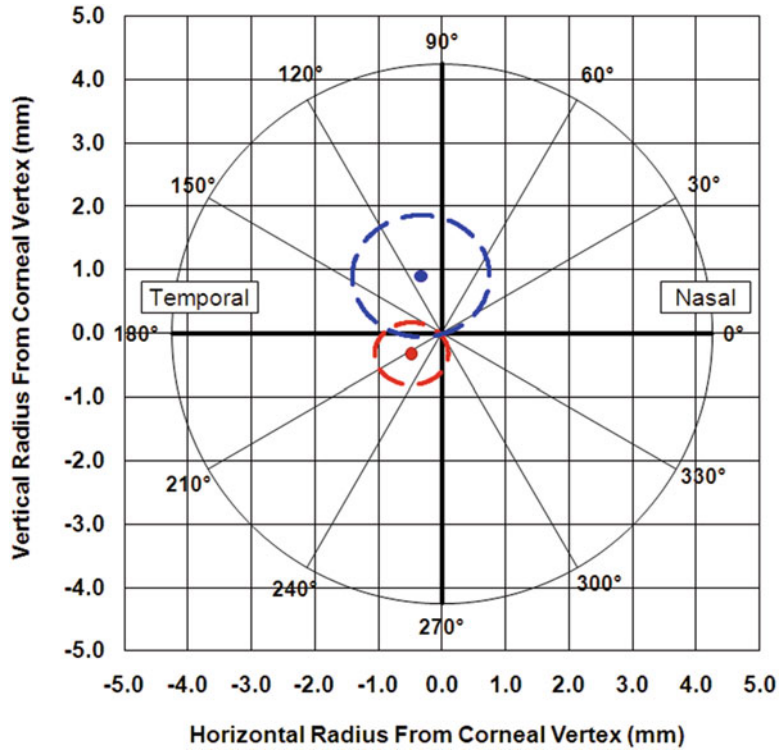

Fig. 13.2 Plot showing the mean location of the thinnest epithelium in a population of 110 normal eyes and 54 keratoconic eyes. The blue dot represents the mean location of the thinnest point for the normal population and the dotted blue line represents one standard deviation. The red dot represents the mean location of the thinnest point for the keratoconic population and the dotted red line represents one standard deviation. *Reprinted with permission from SLACK Incorporated: Reinstein, DZ., Gobbe, M., Archer, T., Silverman, R., Coleman, J. (2010). "Epithelial, Stromal and Total Corneal Thickness in Keratoconus." Journal or Refractive Surgery, 26, 259–271*

the central 5 mm of the cornea was displaced on average 0.33 mm (±1.08) temporally and 0.90 mm (±0.96) superiorly with reference to the corneal vertex (Fig. 13.1).

Figure 13.2a shows a B-scan of a normal cornea. The epithelium appears regular in thickness.

Figure 13.4, Column 1 shows the keratometry, Atlas 995 (Carl Zeiss Meditec, Jena, Germany) corneal topography map and PathFinder™ corneal analysis, Orbscan II (software version 3.00) anterior elevation BFS, Orbscan II posterior elevation BFS and Artemis epithelial thickness profile of a normal eye.

Epithelial thickness can now also be measured using some optical coherence tomography systems, notably the RTVue (Optovue, Fremont, CA) [51–53]. These studies have confirmed this superior–inferior and nasal-temporal asymmetric profile for epithelial thickness in normal eyes [53].

This non-uniformity seems to provide evidence that the epithelial thickness is regulated by eyelid mechanics and blinking, as we suggested in 1994 [50]. We postulated that the eyelid might effectively be chafing the surface epithelium during blinking and that the posterior surface of the semi-rigid tarsus provides a template for the outer shape of the epithelial surface. During blinking, which occurs on average between 300 and 1500 times per hour [54], the vertical traverse of the upper lid is much greater than that of the lower lid. Doane [55] studied the dynamics of eyelid anatomy during blinking and found that

during a blink the descent of the upper eyelid reaches its maximum speed at about the time it crosses the visual axis. As a consequence, it is likely that the eyelid applies more force on the superior than inferior cornea. Similarly, the friction on the cornea during lid closure is likely to be greater temporally than nasally as the outer can thus is higher than the inner can thus (mean intercanthal angle = 3°), and the temporal portion of the lid is higher than the nasal lid (mean upper lid angle = 2.7°) [56]. Therefore, it seems that the nature of the eyelid completely explains the non-uniform epithelial thickness profile of a normal eye.

Further evidence for this theory is provided by the epithelial thickness changes observed in orthokeratology [57]. In orthokeratology, a shaped contact lens is placed on the cornea overnight that sits tightly on the cornea centrally but leaves a gap in the mid-periphery. Therefore, the natural template provided by the posterior surface of the semi-rigid tarsus of the eyelid is replaced by an artificial contact lens template designed to fit tightly to the centre of the cornea and loosely paracentrally. We found significant epithelial thickness changes with central thinning and mid-peripheral thickening showing that the epithelium had remodelled according to the template provided by the contact lens, i.e. the epithelium is chafed and squashed by the lens centrally while the epithelium is free to thicken paracentrally where the lens is not so tightly fitted.

13.4 Epithelial Thickness Profile in Keratoconic Eyes

It is well known that the epithelial thickness changes in keratoconus since extreme steepening leads to epithelial breakdown, as often seen clinically. Epithelial thinning over the cone has been demonstrated using histopathologic analysis of keratoconic corneas by Scroggs et al. [58] and later using custom software and a Humphrey-Zeiss OCT system (Humphrey Systems, Dublin, CA) by Haque et al. [59].

We have characterized the in vivo epithelial thickness profile in a population of keratoconic eyes. The subjects included for the study had previously been diagnosed with keratoconus, and the diagnosis was confirmed by clinical signs of keratoconus such as microscopic signs at the slit-lamp, corneal topographic changes, high refractive astigmatism, reduced best-corrected visual acuity and contrast sensitivity, and significant level of higher order aberrations, in particular vertical coma. We measured the epithelial thickness profile across the central 10 mm diameter of the cornea for 54 keratoconic eyes of 30 patients and averaged the data in the population [60]. Epithelial thickness values for left eyes were reflected in the vertical axis and superimposed onto the right eye values so that nasal/temporal characteristics could be combined.

The average epithelial thickness profile in keratoconus revealed that the epithelium was significantly more irregular in thickness compared to normals. The epithelium was thinnest at the apex of the cone and this thin epithelial zone was surrounded by an annulus of thickened epithelium (Fig. 13.1b). While all eyes exhibited the same epithelial doughnut pattern, characterized by a localized central zone of thinning surrounded by an annulus of thick epithelium, the thickness values of the thinnest point and the thickest point as well as the difference in thickness between the thinnest and thickest epithelium varied greatly between eyes. There was a statistically significant correlation between the thinnest epithelium and the steepest keratometry (D), indicating that as the cornea became steeper, the epithelial thickness minimum became thinner. In addition, there was a statistically significant correlation between the thickness of the thinnest epithelium and the difference in thickness between the thinnest and thickest epithelium. This indicated that as the epithelium thinned, there was an increase in the irregularity of the epithelial thickness profile, i.e. that there was an increase in the severity of the keratoconus. The location of the thinnest epithelium within the central 5 mm of the cornea was displaced on average 0.48 mm (±0.66 mm) tempo-

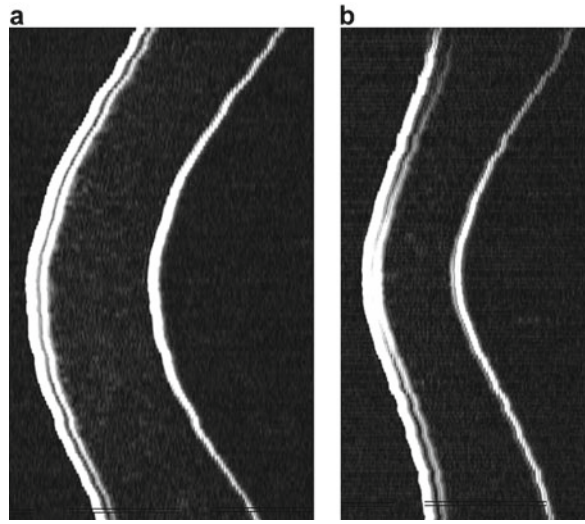

Fig. 13.3 (**a**) (*left*) Horizontal non-geometrically corrected B-scan of a normal cornea obtained using the Artemis very high-frequency digital ultrasound arc scanner. The epithelium appears uniform in thickness across the 10 mm diameter of the scan. (**b**) (*right*) Vertical non-geometrically corrected B-scan of a keratoconic cornea obtained using the Artemis very high-frequency digital ultrasound arc-scanner. The epithelium appears very thin centrally coincident with a visible cone on the back surface. The epithelium is clearly thicker either side of the cone. The central epithelium is much thinner and the peripheral epithelium is much thicker compared to that seen in the normal eye

rally and 0.32 mm (±0.67 mm) inferiorly with reference to the corneal vertex (Fig. 13.2). The mean epithelial thickness for all eyes was 45.7 ± 5.9 μm (range: 33.1–56.3 μm) at the corneal vertex, 38.2 ± 5.8 μm (range: 29.6–52.4 μm) at the thinnest point and 66.8 ± 7.2 μm (range: 54.1–94.4 μm) at the thickest point [60].

Figure 13.3b shows a B-scan for a keratoconic cornea which demonstrates the lack of homogeneity in epithelial thickness as well as central corneal thinning. There is epithelial thinning over the cone and relative epithelial thickening adjacent to the stromal surface cone.

Figure 13.4, Column 2 shows the keratometry, Atlas 995 corneal topography map and PathFinder™ corneal analysis, Orbscan II anterior elevation BFS, Orbscan II posterior elevation BFS and Artemis epithelial thickness profile of a keratoconic eye. As expected, the front surface topography shows infero-temporal steepening with steep average keratometry and high astigmatism; the anterior and posterior elevation BFS maps demonstrate that the apex of the cone is located infero-temporally; the epithelial thickness profile shows epithelial thinning at the apex of the cone surrounded by an annulus of thicker epithelium. The steepest cornea coincides with the apex of the anterior and posterior elevation BFS as well as with the location of the thinnest epithelium.

As for normal eyes, the epithelial thickness profile for keratoconus as described here has been confirmed by studies using OCT [53, 61–63]. The study by Laroche's group [63] elegantly described the different stages of advanced keratoconus demonstrating that as keratoconus moves into its latter stages, a very different epithelial thickness profile becomes apparent. In advanced keratoconus, there is stromal loss often in the location of the cone, for example due to hydrops. This means that rather than the cone being elevated relative to the rest of the stroma, this region is now a depression. Therefore, the epithelium changes from being thinnest over the cone to being thickest in this region, as it is compensating for a depression instead of an elevation (see next section). There can be significant stromal loss in such advanced keratoconus, so the epithelium can be as thick as 200 μm in some cases.

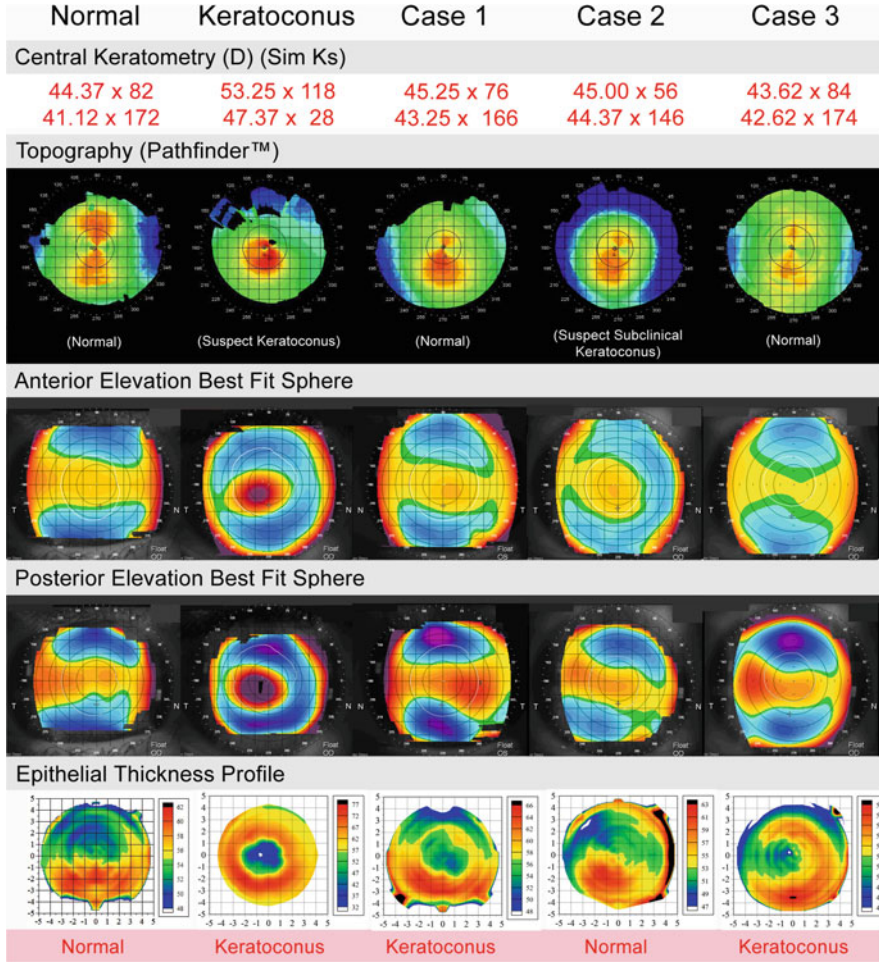

Fig. 13.4 Central keratometry, Atlas corneal topography and PathFinder™ corneal analysis, Orbscan anterior and posterior elevation BFS and Artemis epithelial thickness profile for one normal eye, one keratoconic eye, and three example eyes where the diagnosis of keratoconus might be misleading from topography. The final diagnosis based on the epithelial thickness profile is shown at the bottom of each example. *Reprinted with permission from SLACK Incorporated: Reinstein, DZ., Gobbe, M., Archer, T., Silverman, R., Coleman, J. (2010). "Epithelial, Stromal and Total Corneal Thickness in Keratoconus." Journal or Refractive Surgery, 26, 259–271*

Examples of this epithelial thickening were also reported by Rocha et al. [61] who concluded that focal central epithelial thinning was suggestive but not pathognomonic for keratoconus (i.e. the presence of an epithelial doughnut pattern did not prove beyond any doubt that an eye has keratoconus). However, as described by Laroche, these cases only appear in very advanced keratoconus, which means that they are of no interest with respect to keratoconus screening. Eyes with early keratoconus will never present with epithelial thickening in the location of the cone as by definition if there has been stromal loss, then the keratoconus must be more advanced and the cornea will be obviously abnormal.

13.5 Understanding the Predictable Behaviour of the Corneal Epithelium

Epithelial thickness changes in keratoconus provide another example of the very predictable mechanism of the corneal epithelium to compensate

for irregularities on the stromal surface. Epithelial thickness changes have also been described after myopic excimer laser ablation [64–67], hyperopic excimer laser ablation [68], radial keratotomy [69], intra-corneal ring segments [70], irregularly irregular astigmatism after corneal refractive surgery [45, 71–75] and in ectasia [76].

In all of these cases, the epithelial thickness changes are clearly a compensatory response to the change to the stromal surface and can all be explained by the theory of eyelid template regulation of epithelial thickness [46]. Compensatory epithelial thickness changes can be summarized by the following rules:

1. The epithelium thickens in areas where tissue has been removed or the curvature has been flattened (e.g. central thickening after myopic ablation [64–66] or radial keratotomy [69] and peripheral thickening after hyperopic ablation [68]).
2. The epithelium thins over regions that are relatively elevated or the curvature has been steepened (e.g. central thinning in keratoconus [53, 60–63], ectasia [76] and after hyperopic ablation [68]).
3. The magnitude of epithelial changes correlates to the magnitude of the change in curvature (e.g. more epithelial thickening after higher myopic ablation [64, 65, 67], after higher hyperopic ablation [68] and in more advanced keratoconus [53, 60–63]).
4. The amount of epithelial remodelling is defined by the rate of change of curvature of an irregularity [46, 77]; there will be more epithelial remodelling for a more localized irregularity [45, 72, 73, 75]. The epithelium effectively acts as a low pass filter, smoothing local changes (high curvature gradient) almost completely, but only partially smoothing global changes (low curvature gradient). For example, there is almost twice as much epithelial thickening after a hyperopic ablation [68] compared with a myopic ablation [64, 65, 67], and there is almost total epithelial compensation for small, very localized stromal loss such as after a corneal ulcer [68].

13.6 Diagnosing Early Keratoconus Using Epithelial Thickness Profiles

We have shown that mapping of the epithelial thickness profile reveals a very distinct thickness profile in keratoconus compared to that of normal corneas, due to the compensatory mechanism of the epithelium for stromal irregularities. We have also shown that the epithelial thickness profile changes with the progression of the disease; as the keratoconus becomes more severe, the epithelium at the apex of the cone becomes thinner and the surrounding annulus of epithelium in the epithelial doughnut pattern becomes thicker. Therefore, the degree of epithelial abnormality in both directions (thinner and thicker than normal) can be used to confirm or exclude a diagnosis of keratoconus in eyes suggestive but not conclusive of a diagnosis of keratoconus on topography at a very early stage in the expression of the disease [78].

13.6.1 Pattern of Epithelial Thickness Profile

The epithelial thickness profile in normal eyes demonstrates that the epithelium is on average thicker inferiorly than superiorly and slightly thicker nasally than temporally. There is very little variation in epithelial thickness within both the inferior hemi-cornea and the superior hemi-cornea. In contrast, in keratoconic eyes, the average epithelial thickness map showed an epithelial doughnut pattern characterized by a localized central zone of thinning overlying the stromal cone, surrounded by an annulus of thick epithelium. In early keratoconus, we would expect to see the pattern of localized epithelial thinning surrounded by an annulus of thick epithelium coincident with a suspected cone on posterior elevation BFS. The coincidence of epithelial thinning together with an eccentric posterior elevation BFS apex may reveal whether or not to ascribe significance to an eccentric posterior elevation BFS apex occurring *concurrently with* a

normal front surface topography. In other words, in the presence of normal front surface topography, thinning of the epithelium coincident with the location of the posterior elevation BFS apex would represent total masking or compensation for a sub-surface stromal cone and herald posterior elevation BFS changes which *do* represent keratoconus. Conversely, finding thicker epithelium over an area of topographic steepening or an eccentric posterior elevation BFS apex would imply that the steepening is *not* due to a keratoconic sub-surface stromal cone, but more likely due to localized epithelial thickening. Localized compensatory changes in epithelial thickness profiles can be detected by Artemis VHF digital ultrasound once they exceed 1–2 μm. In a way, examination of epithelial thickness profile irregularities provides a very sensitive method of examining stromal surface topography—by proxy. Therefore, this technique provides increased sensitivity and specificity to a diagnosis of keratoconus well in advance of any detectable corneal front surface topographic change.

Case Examples

Figure 13.4 shows three selected examples where epithelial thickness profiles helped to interpret and diagnose anterior and posterior elevation BFS abnormalities. In each case, the epithelial thickness profile appears to be able to differentiate cases where the diagnosis of keratoconus is uncertain, from normal [78].

Case 1 (OS) represents a 25-year-old male, with a manifest refraction of −1.00 −0.50 × 150 and a best spectacle-corrected visual acuity of 20/16. Atlas corneal topography demonstrated inferior steepening which would traditionally indicate keratoconus. The keratometry was 45.25/43.25 D × 76, and PathFinder™ corneal analysis classified the topography as normal. Orbscan II posterior elevation BFS showed that the posterior elevation BFS apex was decentred infero-temporally. Corneal pachymetry minimum by handheld ultrasound was 479 μm. Contrast sensitivity was slightly below the normal range measured using the CSV-1000 (Vector Vision Inc., Greenville, Ohio). There was –0.30 μm (OSA notation) of vertical coma on WASCA aberrometry. Corneal hysteresis was 7.5 mmHg and corneal resistance factor was 7.1 mmHg, which are low, but these could be affected by the low corneal thickness. The combination of inferior steepening, an eccentric posterior elevation BFS apex and thin cornea raised the suspicion of keratoconus although there was no suggestion of keratoconus by refraction, keratometry or PathFinder™ corneal analysis. Artemis epithelial thickness profile showed a pattern typical of keratoconus with an epithelial doughnut shape characterized by a localized zone of epithelial thinning displaced infero-temporally over the eccentric posterior elevation BFS apex, surrounded by an annulus of thick epithelium. The coincidence of an area of epithelial thinning with the apex of the posterior elevation BFS, as well as the increased irregularity of the epithelium confirmed the diagnosis of early keratoconus.

Case 2 (OD) represents a 31-year-old female, with a manifest refraction of –2.25 –0.50 × 88 and a best spectacle-corrected visual acuity of 20/16. Atlas corneal topography demonstrated a very similar pattern to case 1 of inferior steepening, therefore suggesting that the eye could also be keratoconic. The keratometry was 44.12/44.75 D × 148, and PathFinder™ corneal analysis classified the topography as suspect subclinical keratoconus. Orbscan II posterior elevation BFS showed that the apex was slightly decentred nasally. Corneal pachymetry minimum by handheld ultrasound was 538 μm. Contrast sensitivity was in the normal range. There was 0.32 μm (OSA notation) of vertical coma on WASCA aberrometry. Corneal hysteresis was 10.1 mmHg and corneal resistance factor was 9.8 mmHg, which are well within normal range. The combination of inferior steepening, against-the-rule astigmatism and high degree of vertical coma raised the suspicion of keratoconus, which was also noted by PathFinder™ corneal analysis. Artemis epithelial thickness profile showed a typical normal pattern with thicker epithelium inferiorly and thinner epithelium superiorly. Thicker epithelium inferiorly over the suspected cone (inferior steepening on topography) was inconsistent with an underlying stromal surface cone, and therefore the diagno-

sis of keratoconus was excluded. This patient would have been rejected for surgery given a documented PathFinder™ corneal analysis warning of suspect subclinical keratoconus, but given the epithelial thickness profile, this patient was deemed a suitable candidate for LASIK.

The anterior corneal topography in case 3 (OD) bears no features related to keratoconus. The patient is a 35-year-old female with a manifest refraction of −25 −0.50×4 and a best spectacle-corrected visual acuity of 20/16. The refraction had been stable for at least 10 years and the contrast sensitivity was within normal limits. The keratometry was 43.62/42.62 D×74 and PathFinder™ analysis classified the topography as normal. Orbscan II posterior elevation BFS showed that the apex was slightly decentred infero-temporally, but the anterior elevation BFS apex was well centred. Corneal pachymetry minimum by handheld ultrasound was 484 μm. Pentacam (Oculus, Wetzlar, Germany) keratoconus screening indices were normal. WASCA ocular higher order aberrations were low (RMS = 0.19 μm) as well as the level of vertical coma (coma = 0.066 μm). Corneal hysteresis was 8.9 mmHg and corneal resistance factor was 8.8 mmHg, both within normal limits. In this case, only the slightly eccentric posterior elevation BFS apex and the low–normal corneal thickness were suspicious for keratoconus, while all other screening methods gave no indication of keratoconus. However, the epithelial thickness profile showed an epithelial doughnut pattern characterized by localized epithelial thinning surrounded by an annulus of thick epithelium, coincident with the eccentric posterior elevation BFS apex. Epithelial thinning with surrounding annular thickening over the eccentric posterior elevation BFS apex indicated the presence of probable sub-surface keratoconus. In this case, it seems that the epithelium had fully compensated for the stromal surface irregularity so that the anterior surface topography of the cornea appeared perfectly regular. Given the regularity of the front surface topography and the normality of nearly all other screening parameters, it is feasible that this patient could have been deemed suitable for corneal refractive surgery and subsequently developed ectasia. As we were able to also consider the epithelial thickness profile, this patient was rejected for corneal refractive surgery. This kind of case may explain some reported cases of ectasia "without a cause" [79].

13.7 Automated Algorithm for Classification by Epithelium

Based on this qualitative diagnostic method, we then set out to derive an automated classifier to detect keratoconus using epithelial thickness data, together with Ron Silverman and his group at Columbia University [80]. We used stepwise linear discriminant analysis (LDA) and neural network (NN) analysis to develop multivariate models based on combinations of 161 features comparing a population of 130 normal and 74 keratoconic eyes. This process resulted in a six-variable model that provided an area under the receiver operating curve of 100 %, indicative of complete separation of keratoconic from normal corneas. Test-set performance averaged over ten trials, gave a specificity of 99.5 ± 1.5 % and sensitivity of 98.9 ± 1.9 %. Maps of the average epithelium and LDA function values were also found to be well correlated with keratoconus severity grade (see Figs. 13.5 and 13.6). Other groups have also been working on automated classification algorithms based on epithelial thickness data obtained by OCT [53, 81].

Following this study, we then applied the algorithm to a population of 10 patients with unilateral keratoconus (clinically and algorithmically topographically normal in the fellow eyes), on the basis that the fellow eye in such patients represents a latent form of keratoconus, and as such, has been considered a gold standard for studies aimed at early keratoconus detection. These eyes were also analysed using the Belin-Ambrosio enhanced ectasia display (BAD-D parameter and ART-Max) [20, 24, 82] and the Orbscan SCORE value as described by Saad and Gatinel [28–30].

Table 1 summarizes the diagnosis derived for the fellow eyes using the classification function

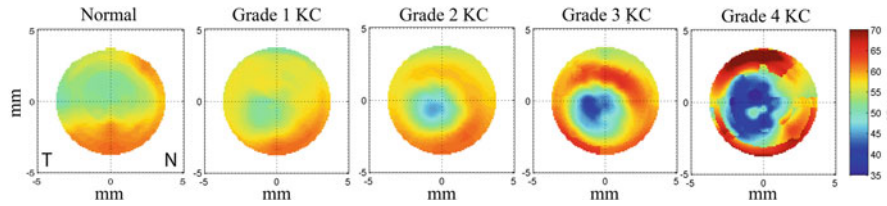

Fig. 13.5 Epithelial thickness maps averaged over all normal corneas and for each keratoconus grade. The departure from the normal epithelial distribution is evident even in grade 1 keratoconus but becomes more obvious with severity. *Reprinted with permission from IOVS: Silverman RH, Urs R, Roychoudhury A, Archer TJ, Gobbe M, Reinstein DZ. Epithelial remodeling as basis for machine-based identification of keratoconus. Invest Ophthalmol Vis Sci. 2014 Mar 13;55(3):1580–7*

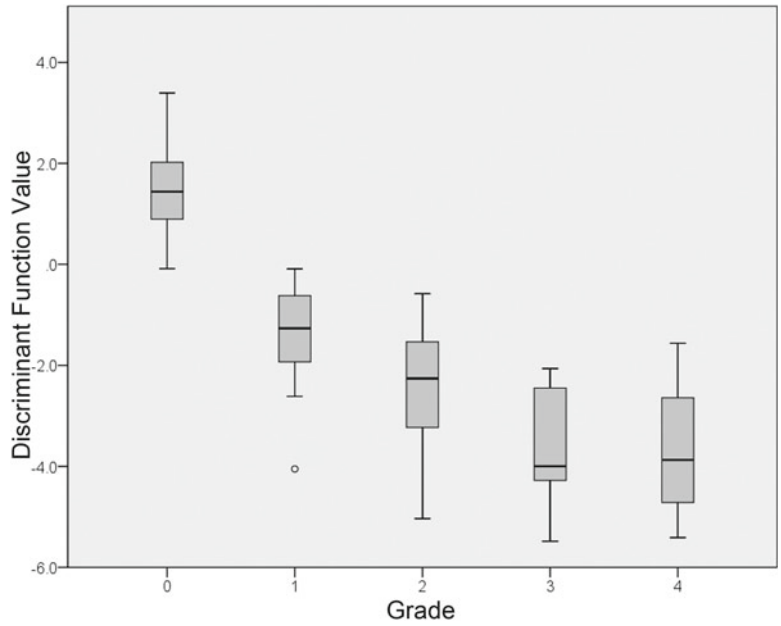

Fig. 13.6 Box and whisker plot of discriminant function value versus keratoconus severity grade. Grade 0 represents normal subjects. Grades 1–4 are based on Krumeich classification. Boxes represent ±1 quartile about median value (*horizontal line*), and whiskers represent full range of values for each group. *Circles* indicate outliers. *Reprinted with permission from IOVS: Silverman RH, Urs R, Roychoudhury A, Archer TJ, Gobbe M, Reinstein DZ. Epithelial remodeling as basis for machine-based identification of keratoconus. Invest Ophthalmol Vis Sci. 2014 Mar 13;55(3):1580–7*

based on epithelial thickness parameters, the classification function combining VHF digital ultrasound (epithelial and stromal thickness) and Pentacam HD parameters, the BAD-D and ART-Max values, and the Orbscan SCORE value. The last column of the table indicates whether the topographic map displayed suspicious features of keratoconus such as inferior steepening and asymmetric bow-tie. The table also shows the percentage of eyes that were classified as keratoconus by each method.

The most interesting finding of this study was that more than 50 % of the fellow eyes were classified as normal by all methods. This was similar to the result reported by Bae et al. [26], who found no difference in the BAD-D or ART-Max values between normal and topographically normal fellow eyes of keratoconus patients. This is in con-

trast to other studies using unilateral keratoconus populations where a much higher sensitivity was reported; however, these studies often included patients with a suspicious topography in the fellow eye (i.e. some studies use a more rigorous definition of unilateral keratoconus than others) [27]. Therefore, the main conclusion from the study was to put into question the validity of using unilateral keratoconus patients for keratoconus screening studies. The fact that a number of these fellow eyes showed absolutely no indication of keratoconus by any method implies that it is likely that these were truly normal eyes. However, it is generally agreed that keratoconus as a disease must be bilateral [83], therefore it appears that these cases are patients who do not have keratoconus, but have induced an ectasia in one eye, for example by eye rubbing or trauma. This means that using "unilateral keratoconus" populations to study keratoconus screening may be flawed.

The alternative is somewhat more alarming, as this would mean that there are eyes with keratoconus that are literally undetectable by any existing method. This would, however, explain any case of "ectasia without a cause" [79, 84]. Detection of keratoconus in such cases may require development of new in vivo measurements of corneal biomechanics, although this appears to be outside the scope of current methods such as the Ocular Response Analyzer [85–87] and Corvis (Oculus, Wetzlar, Germany) [86, 87] due to the wide scatter in the data acquired. Another factor, as has been described using Brillouin microscopy [88], may be that the biomechanical tensile strength of the cornea may not be different from normal in early keratoconus when measuring the whole cornea globally, but there may only be a difference in the region localized of the cone (or in the location of a future cone). Another potential and final solution would be whether a genotype or other molecular marker for keratoconus could be found [89–91].

Finally, another interpretation of this result is that keratoconus may not necessarily be a disease of abnormal stromal substance. The localization of the reduced corneal biomechanics found in keratoconus suggests that this may be caused by a local defect in Bowman's layer due to eye rubbing or other trauma. A break in Bowman's layer would reduce the tension locally and the asymmetric stress concentration would then cause the stroma to bulge in this location. Evidence for changes in Bowman's layer in keratoconus has been reported using ultra-high resolution OCT; Shousha et al. [92] showed that Bowman's layer was thinner inferiorly in keratoconus and described a Bowman's ectasia index (BEI) to use for keratoconus screening. Yadav et al. [93] also described differences in the thickness of Bowman's layer in keratoconus, as well as a difference in light scatter.

13.8 Conclusion

We have demonstrated that the epithelial thickness profile was significantly different between normal eyes and keratoconic eyes. Whereas the epithelium in normal eyes was relatively homogeneous in thickness with a pattern of slightly thicker epithelium inferiorly than superiorly, the epithelium in keratoconic eyes was irregular showing a doughnut shaped pattern, and a marked difference in thickness between the thin epithelium at the centre of the doughnut and the surrounding annulus of thick epithelium. We have shown that the epithelial thickness profile progresses along with the evolution of keratoconus. More advanced keratoconus produces more irregularity in the epithelial thickness profile. We have found that the distinctive epithelial doughnut pattern associated with keratoconus can be used to confirm or exclude the presence of an underlying stromal surface cone in cases with normal or suspect front surface topography as well as being a "qualifier" for the finding of an eccentric posterior elevation BFS apex.

Knowledge of the differences in epithelial thickness profile between the normal population and the keratoconic population allowed us to identify several features of the epithelial thickness profile that might help to discriminate between normal eyes and keratoconus suspect eyes. We developed an automated classifier based on these features that provides good sensitivity and specificity for keratoconus diagnosis.

Randleman, in his paper assessing risk factors for ectasia reported that ectasia might still occur after uncomplicated surgery in appropriately screened candidates [33]. Mapping of epithelial thickness profiles might provide an explanation for these cases; it could be that a stromal surface cone was masked by epithelial compensation and the front surface topography appeared normal.

Mapping of the epithelial thickness profile may increase sensitivity and specificity of screening for keratoconus compared to current conventional corneal topographic screening alone and may be useful in clinical practice in two very important ways.

Firstly, epithelial thickness mapping can exclude the appropriate patients by detecting keratoconus earlier or confirming keratoconus in cases where topographic changes may be clinically judged as being "within normal limits". Epithelial information allows an earlier diagnosis of keratoconus as epithelial changes will occur before changes on the front surface of the cornea become apparent. Epithelial thinning coincident with an eccentric posterior elevation BFS apex, and in particular if surrounded by an annulus of thicker epithelium is consistent with keratoconus. Excluding early keratoconic patients from laser refractive surgery will reduce and potentially eliminate the risk of iatrogenic ectasia of this aetiology and therefore increase the safety of laser refractive surgery. From our data, 136 eyes out of 1532 consecutive myopic eyes screened for refractive surgery demonstrated abnormal topography suspect of keratoconus. All 136 eyes were screened with Artemis VHF digital ultrasound arc scanning and individual epithelial thickness profiles were mapped. Out of 136 eyes with suspect keratoconus, only 22 eyes (16%) were confirmed as keratoconus [94].

Second, epithelial thickness profiles may be useful in excluding a diagnosis of keratoconus despite suspect topography. Epithelial thickening over an area of topographic steepening implies that the steepening is not due to an underlying ectatic surface. In such cases, excluding keratoconus using epithelial thickness profiles appears to allow patients who otherwise would have been denied treatment due to suspect topography to be deemed suitable for surgery. From our data, out of the 136 eyes with suspect keratoconus screened with Artemis VHF digital ultrasound arc scanning, 114 eyes (84%) showed normal epithelial thickness profile and were diagnosed as non-keratoconic and deemed suitable for corneal refractive surgery. One year post-LASIK follow-up data [94] and preliminary 2-years follow-up data [95] on these demonstrated equal stability and refractive outcomes as matched control eyes.

In summary, epithelial thickness mapping appears to be a new and useful tool for aiding in the diagnosis of keratoconus when topographical changes are equivocal.

Compliance with Ethical Requirements Dr. Reinstein is a consultant for Carl Zeiss Meditec (Jena, Germany). Drs Reinstein and Silverman have a proprietary interest in the Artemis technology (ArcScan Inc., Golden, Colorado) and are authors of patents related to VHF digital ultrasound administered by the Center for Technology Licensing at Cornell University, Ithaca, New York. Timothy Archer, Marine Gobbe, and Raksha Urs declare that they have no conflict of interest.

Informed Consent: All procedures followed were in accordance with the ethical standards of the responsible committee on human experimentation (institutional and national) and with the Helsinki Declaration of 1975, as revised in 2000. Informed consent was obtained from all patients for being included in the study.

No animal studies were carried out by the authors for this chapter.

References

1. Ambrosio Jr R, Wilson SE. Complications of laser in situ keratomileusis: etiology, prevention, and treatment. J Refract Surg. 2001;17(3):350–79.
2. Seiler T, Koufala K, Richter G. Iatrogenic keratectasia after laser in situ keratomileusis. J Refract Surg. 1998;14(3):312–7.
3. Krachmer JH, Feder RF, Belin MW. Keratoconus and related non-inflammatory corneal thinning disorders. Surv Ophthalmol. 1984;28:293–322.
4. Wilson SE, Klyce SD. Screening for corneal topographic abnormalities before refractive surgery. Ophthalmology. 1994;101(1):147–52.
5. Klyce SD. Computer-assisted corneal topography. High-resolution graphic presentation and analysis of keratoscopy. Invest Ophthalmol Vis Sci. 1984;25(12):1426–35.
6. Rabinowitz YS, Yang H, Brickman Y, Akkina J, Riley C, Rotter JI, et al. Videokeratography database of normal human corneas. Br J Ophthalmol. 1996;80(7):610–6.

7. Rabinowitz YS, McDonnell PJ. Computer-assisted corneal topography in keratoconus. Refract Corneal Surg. 1989;5(6):400–8.
8. Rabinowitz YS. Videokeratographic indices to aid in screening for keratoconus. J Refract Surg. 1995;11(5):371–9.
9. Rabinowitz YS. Tangential vs sagittal videokeratographs in the "early" detection of keratoconus. Am J Ophthalmol. 1996;122(6):887–9.
10. Rabinowitz YS, Rasheed K. KISA% index: a quantitative videokeratography algorithm embodying minimal topographic criteria for diagnosing keratoconus. J Cataract Refract Surg. 1999;25(10):1327–35.
11. Smolek MK, Klyce SD. Current keratoconus detection methods compared with a neural network approach. Invest Ophthalmol Vis Sci. 1997;38(11):2290–9.
12. Maeda N, Klyce SD, Smolek MK. Comparison of methods for detecting keratoconus using videokeratography. Arch Ophthalmol. 1995;113(7):870–4.
13. Nesburn AB, Bahri S, Salz J, Rabinowitz YS, Maguen E, Hofbauer J, et al. Keratoconus detected by videokeratography in candidates for photorefractive keratectomy. J Refract Surg. 1995;11(3):194–201.
14. Chastang PJ, Borderie VM, Carvajal-Gonzalez S, Rostene W, Laroche L. Automated keratoconus detection using the EyeSys videokeratoscope. J Cataract Refract Surg. 2000;26(5):675–83.
15. Maeda N, Klyce SD, Smolek MK, Thompson HW. Automated keratoconus screening with corneal topography analysis. Invest Ophthalmol Vis Sci. 1994;35(6):2749–57.
16. Kalin NS, Maeda N, Klyce SD, Hargrave S, Wilson SE. Automated topographic screening for keratoconus in refractive surgery candidates. Clao J. 1996; 22(3):164–7.
17. Auffarth GU, Wang L, Volcker HE. Keratoconus evaluation using the Orbscan Topography System. J Cataract Refract Surg. 2000;26(2):222–8.
18. Rao SN, Raviv T, Majmudar PA, Epstein RJ. Role of Orbscan II in screening keratoconus suspects before refractive corneal surgery. Ophthalmology. 2002; 109(9):1642–6.
19. Tomidokoro A, Oshika T, Amano S, Higaki S, Maeda N, Miyata K. Changes in anterior and posterior corneal curvatures in keratoconus. Ophthalmology. 2000;107(7):1328–32.
20. Ambrosio Jr R, Alonso RS, Luz A, Coca Velarde LG. Corneal-thickness spatial profile and corneal-volume distribution: tomographic indices to detect keratoconus. J Cataract Refract Surg. 2006;32(11):1851–9.
21. de Sanctis U, Loiacono C, Richiardi L, Turco D, Mutani B, Grignolo FM. Sensitivity and specificity of posterior corneal elevation measured by Pentacam in discriminating keratoconus/subclinical keratoconus. Ophthalmology. 2008;115(9):1534–9.
22. Saad A, Gatinel D. Evaluation of total and corneal wavefront high order aberrations for the detection of forme fruste keratoconus. Invest Ophthalmol Vis Sci. 2012;53(6):2978–92.
23. Luce DA. Determining in vivo biomechanical properties of the cornea with an ocular response analyzer. J Cataract Refract Surg. 2005;31(1):156–62.
24. Ambrosio Jr R, Caiado AL, Guerra FP, Louzada R, Roy AS, Luz A, et al. Novel pachymetric parameters based on corneal tomography for diagnosing keratoconus. J Refract Surg. 2011;27(10):753–8.
25. Fontes BM, Ambrosio Jr R, Salomao M, Velarde GC, Nose W. Biomechanical and tomographic analysis of unilateral keratoconus. J Refract Surg. 2010;26(9):677–81.
26. Bae GH, Kim JR, Kim CH, Lim DH, Chung ES, Chung TY. Corneal topographic and tomographic analysis of fellow eyes in unilateral keratoconus patients using Pentacam. Am J Ophthalmol. 2014;157(1):103–9. e1.
27. Muftuoglu O, Ayar O, Ozulken K, Ozyol E, Akinci A. Posterior corneal elevation and back difference corneal elevation in diagnosing forme fruste keratoconus in the fellow eyes of unilateral keratoconus patients. J Cataract Refract Surg. 2013;39(9):1348–57.
28. Chan C, Ang M, Saad A, Chua D, Mejia M, Lim L, et al. Validation of an objective scoring system for forme fruste keratoconus detection and post-LASIK ectasia risk assessment in Asian eyes. Cornea. 2015;34(9):996–1004.
29. Saad A, Gatinel D. Validation of a new scoring system for the detection of early forme of keratoconus. Int J Kerat Ect Cor Dis. 2012;1(2):100–8.
30. Saad A, Gatinel D. Topographic and tomographic properties of forme fruste keratoconus corneas. Invest Ophthalmol Vis Sci. 2010;51(11):5546–55.
31. Mahmoud AM, Nunez MX, Blanco C, Koch DD, Wang L, Weikert MP, et al. Expanding the cone location and magnitude index to include corneal thickness and posterior surface information for the detection of keratoconus. Am J Ophthalmol. 2013;156(6):1102–11.
32. Randleman JB, Trattler WB, Stulting RD. Validation of the ectasia risk score system for preoperative laser in situ keratomileusis screening. Am J Ophthalmol. 2008;145(5):813–8.
33. Randleman JB, Woodward M, Lynn MJ, Stulting RD. Risk assessment for ectasia after corneal refractive surgery. Ophthalmology. 2008;115(1):37–50.
34. Seiler T, Quurke AW. Iatrogenic keratectasia after LASIK in a case of forme fruste keratoconus. J Cataract Refract Surg. 1998;24(7):1007–9.
35. Speicher L, Gottinger W. Progressive corneal ectasia after laser in situ keratomileusis (LASIK). Klin Monatsbl Augenheilkd. 1998;213(4):247–51.
36. Geggel HS, Talley AR. Delayed onset keratectasia following laser in situ keratomileusis. J Cataract Refract Surg. 1999;25(4):582–6.
37. Amoils SP, Deist MB, Gous P, Amoils PM. Iatrogenic keratectasia after laser in situ keratomileusis for less than −4.0 to −7.0 diopters of myopia. J Cataract Refract Surg. 2000;26(7):967–77.
38. McLeod SD, Kisla TA, Caro NC, McMahon TT. Iatrogenic keratoconus: corneal ectasia following laser

in situ keratomileusis for myopia. Arch Ophthalmol. 2000;118(2):282–4.
39. Holland SP, Srivannaboon S, Reinstein DZ. Avoiding serious corneal complications of laser assisted in situ keratomileusis and photorefractive keratectomy. Ophthalmology. 2000;107(4):640–52.
40. Schmitt-Bernard CF, Lesage C, Arnaud B. Keratectasia induced by laser in situ keratomileusis in keratoconus. J Refract Surg. 2000;16(3):368–70.
41. Rao SN, Epstein RJ. Early onset ectasia following laser in situ keratomileusus: case report and literature review. J Refract Surg. 2002;18(2):177–84.
42. Malecaze F, Coullet J, Calvas P, Fournie P, Arne JL, Brodaty C. Corneal ectasia after photorefractive keratectomy for low myopia. Ophthalmology. 2006;113(5):742–6.
43. Randleman JB, Russell B, Ward MA, Thompson KP, Stulting RD. Risk factors and prognosis for corneal ectasia after LASIK. Ophthalmology. 2003; 110(2):267–75.
44. Leccisotti A. Corneal ectasia after photorefractive keratectomy. Graefes Arch Clin Exp Ophthalmol. 2007;245(6):869–75.
45. Reinstein DZ, Archer T. Combined Artemis very high-frequency digital ultrasound-assisted transepithelial phototherapeutic keratectomy and wavefront-guided treatment following multiple corneal refractive procedures. J Cataract Refract Surg. 2006;32(11):1870–6.
46. Reinstein DZ, Archer TJ, Gobbe M. Rate of change of curvature of the corneal stromal surface drives epithelial compensatory changes and remodeling. J Refract Surg. 2014;30(12):800–2.
47. Reinstein DZ, Silverman RH, Trokel SL, Coleman DJ. Corneal pachymetric topography. Ophthalmology. 1994;101(3):432–8.
48. Reinstein DZ, Silverman RH, Raevsky T, Simoni GJ, Lloyd HO, Najafi DJ, et al. Arc-scanning very high-frequency digital ultrasound for 3D pachymetric mapping of the corneal epithelium and stroma in laser in situ keratomileusis. J Refract Surg. 2000;16(4):414–30.
49. Reinstein DZ, Archer TJ, Gobbe M, Silverman RH, Coleman DJ. Epithelial thickness in the normal cornea: three-dimensional display with Artemis very high-frequency digital ultrasound. J Refract Surg. 2008;24(6):571–81.
50. Reinstein DZ, Silverman RH, Coleman DJ. High-frequency ultrasound measurement of the thickness of the corneal epithelium. Refract Corneal Surg. 1993;9(5):385–7.
51. Prakash G, Agarwal A, Mazhari AI, Chari M, Kumar DA, Kumar G, et al. Reliability and reproducibility of assessment of corneal epithelial thickness by fourier domain optical coherence tomography. Invest Ophthalmol Vis Sci. 2012;53(6):2580–5.
52. Ge L, Shen M, Tao A, Wang J, Dou G, Lu F. Automatic segmentation of the central epithelium imaged with three optical coherence tomography devices. Eye Contact Lens. 2012;38(3):150–7.
53. Li Y, Tan O, Brass R, Weiss JL, Huang D. Corneal epithelial thickness mapping by Fourier-domain optical coherence tomography in normal and keratoconic eyes. Ophthalmology. 2012;119(12):2425–33.
54. Bentivoglio AR, Bressman SB, Cassetta E, Carretta D, Tonali P, Albanese A. Analysis of blink rate patterns in normal subjects. Mov Disord. 1997;12(6):1028–34.
55. Doane MG. Interactions of eyelids and tears in corneal wetting and the dynamics of the normal human eyeblink. Am J Ophthalmol. 1980;89(4):507–16.
56. Young G, Hunt C, Covey M. Clinical evaluation of factors influencing toric soft contact lens fit. Optom Vis Sci. 2002;79(1):11–9.
57. Reinstein DZ, Gobbe M, Archer TJ, Couch D, Bloom B. Epithelial, stromal, and corneal pachymetry changes during orthokeratology. Optom Vis Sci. 2009;86(8):E1006–14.
58. Scroggs MW, Proia AD. Histopathological variation in keratoconus. Cornea. 1992;11(6):553–9.
59. Haque S, Simpson T, Jones L. Corneal and epithelial thickness in keratoconus: a comparison of ultrasonic pachymetry, Orbscan II, and optical coherence tomography. J Refract Surg. 2006;22(5):486–93.
60. Reinstein DZ, Archer TJ, Gobbe M, Silverman RH, Coleman DJ. Epithelial, stromal and corneal thickness in the keratoconic cornea: three-dimensional display with Artemis very high-frequency digital ultrasound. J Refract Surg. 2010;26(4):259–71.
61. Rocha KM, Perez-Straziota CE, Stulting RD, Randleman JB. SD-OCT analysis of regional epithelial thickness profiles in keratoconus, postoperative corneal ectasia, and normal eyes. J Refract Surg. 2013;29(3):173–9.
62. Kanellopoulos AJ, Aslanides IM, Asimellis G. Correlation between epithelial thickness in normal corneas, untreated ectatic corneas, and ectatic corneas previously treated with CXL; is overall epithelial thickness a very early ectasia prognostic factor? Clin Ophthalmol. 2012;6:789–800.
63. Sandali O, El Sanharawi M, Temstet C, Hamiche T, Galan A, Ghouali W, et al. Fourier-domain optical coherence tomography imaging in keratoconus: a corneal structural classification. Ophthalmology. 2013;120(12):2403–12.
64. Gauthier CA, Holden BA, Epstein D, Tengroth B, Fagerholm P, Hamberg-Nystrom H. Role of epithelial hyperplasia in regression following photorefractive keratectomy. Br J Ophthalmol. 1996;80(6): 545–8.
65. Reinstein DZ, Srivannaboon S, Gobbe M, Archer TJ, Silverman RH, Sutton H, et al. Epithelial thickness profile changes induced by myopic LASIK as measured by Artemis very high-frequency digital ultrasound. J Refract Surg. 2009;25(5):444–50.
66. Reinstein DZ, Archer TJ, Gobbe M. Change in epithelial thickness profile 24 hours and longitudinally for 1 year after myopic LASIK: three-dimensional display with Artemis very high-frequency digital ultrasound. J Refract Surg. 2012;28(3):195–201.
67. Kanellopoulos AJ, Asimellis G. Longitudinal postoperative Lasik epithelial thickness profile changes in correlation with degree of myopia correction. J Refract Surg. 2014;30(3):166–71.

68. Reinstein DZ, Archer TJ, Gobbe M, Silverman RH, Coleman DJ. Epithelial thickness after hyperopic LASIK: three-dimensional display with Artemis very high-frequency digital ultrasound. J Refract Surg. 2010;26(8):555–64.
69. Reinstein DZ, Archer TJ, Gobbe M. Epithelial thickness up to 26 years after radial keratotomy: three-dimensional display with Artemis very high-frequency digital ultrasound. J Refract Surg. 2011;27(8):618–24.
70. Reinstein DZ, Srivannaboon S, Holland SP. Epithelial and stromal changes induced by intacs examined by three-dimensional very high-frequency digital ultrasound. J Refract Surg. 2001;17(3):310–8.
71. Reinstein DZ, Silverman RH, Sutton HF, Coleman DJ. Very high-frequency ultrasound corneal analysis identifies anatomic correlates of optical complications of lamellar refractive surgery: anatomic diagnosis in lamellar surgery. Ophthalmology. 1999;106(3):474–82.
72. Reinstein DZ, Archer TJ, Gobbe M. Refractive and topographic errors in topography-guided ablation produced by epithelial compensation predicted by three-dimensional Artemis very high-frequency digital ultrasound stromal and epithelial thickness mapping. J Refract Surg. 2012;28(9):657–63.
73. Reinstein DZ, Archer TJ, Gobbe M. Improved effectiveness of trans-epithelial phototherapeutic keratectomy versus topography-guided ablation degraded by epithelial compensation on irregular stromal surfaces [plus video]. J Refract Surg. 2013;29(8):526–33.
74. Reinstein DZ, Gobbe M, Archer TJ, Youssefi G, Sutton HF. Stromal surface topography-guided custom ablation as a repair tool for corneal irregular astigmatism. J Refract Surg. 2015;31(1):54–9.
75. Reinstein DZ, Archer TJ, Dickeson ZI, Gobbe M. Trans-epithelial phototherapeutic keratectomy protocol for treating irregular astigmatism based population on epithelial thickness measurements by Artemis very high-frequency digital ultrasound. J Refract Surg. 2014;30(6):380–7.
76. Reinstein DZ, Gobbe M, Archer TJ, Couch D. Epithelial thickness profile as a method to evaluate the effectiveness of collagen cross-linking treatment after corneal ectasia. J Refract Surg. 2011;27(5):356–63.
77. Vinciguerra P, Roberts CJ, Albe E, Romano MR, Mahmoud A, Trazza S, et al. Corneal curvature gradient map: a new corneal topography map to predict the corneal healing process. J Refract Surg. 2014;30(3):202–7.
78. Reinstein DZ, Archer TJ, Gobbe M. Corneal epithelial thickness profile in the diagnosis of keratoconus. J Refract Surg. 2009;25(7):604–10.
79. Klein SR, Epstein RJ, Randleman JB, Stulting RD. Corneal ectasia after laser in situ keratomileusis in patients without apparent preoperative risk factors. Cornea. 2006;25(4):388–403.
80. Silverman RH, Urs R, Roychoudhury A, Archer TJ, Gobbe M, Reinstein DZ. Epithelial remodeling as basis for machine-based identification of keratoconus. Invest Ophthalmol Vis Sci. 2014;55(3):1580–7.
81. Temstet C, Sandali O, Bouheraoua N, Hamiche T, Galan A, El Sanharawi M, et al. Corneal epithelial thickness mapping using Fourier-domain optical coherence tomography for detection of form fruste keratoconus. J Cataract Refract Surg. 2015;41(4):812–20.
82. Ambrosio Jr R, Faria-Correia F, Ramos I, Valbon BF, Lopes B, Jardim D, et al. Enhanced screening for ectasia susceptibility among refractive candidates: the role of corneal tomography and biomechanics. Curr Ophthalmol Rep. 2013;1(1):28–38.
83. Gomes JA, Tan D, Rapuano CJ, Belin MW, Ambrosio Jr R, Guell JL, et al. Global consensus on keratoconus and ectatic diseases. Cornea. 2015;34(4):359–69.
84. Ambrosio Jr R, Dawson DG, Salomao M, Guerra FP, Caiado AL, Belin MW. Corneal ectasia after LASIK despite low preoperative risk: tomographic and biomechanical findings in the unoperated, stable, fellow eye. J Refract Surg. 2010;26(11):906–11.
85. Reinstein DZ, Gobbe M, Archer TJ. Ocular biomechanics: measurement parameters and terminology. J Refract Surg. 2011;27(6):396–7.
86. Vellara HR, Patel DV. Biomechanical properties of the keratoconic cornea: a review. Clin Exp Optom. 2015;98(1):31–8.
87. Pinero DP, Alcon N. Corneal biomechanics: a review. Clin Exp Optom. 2014;98:107–16.
88. Scarcelli G, Besner S, Pineda R, Yun SH. Biomechanical characterization of keratoconus corneas ex vivo with Brillouin microscopy. Invest Ophthalmol Vis Sci. 2014;55(7):4490–5.
89. Abu-Amero KK, Al-Muammar AM, Kondkar AA. Genetics of keratoconus: where do we stand? J Ophthalmol. 2014;2014:641708.
90. Burdon KP, Vincent AL. Insights into keratoconus from a genetic perspective. Clin Exp Optom. 2013;96(2):146–54.
91. Rabinowitz YS, Dong L, Wistow G. Gene expression profile studies of human keratoconus cornea for NEIBank: a novel cornea-expressed gene and the absence of transcripts for aquaporin 5. Invest Ophthalmol Vis Sci. 2005;46(4):1239–46.
92. Abou Shousha M, Perez VL, Fraga Santini Canto AP, Vaddavalli PK, Sayyad FE, Cabot F, et al. The use of Bowman's layer vertical topographic thickness map in the diagnosis of keratoconus. Ophthalmology. 2014;121(5):988–93.
93. Yadav R, Kottaiyan R, Ahmad K, Yoon G. Epithelium and Bowman's layer thickness and light scatter in keratoconic cornea evaluated using ultrahigh resolution optical coherence tomography. J Biomed Opt. 2012;17(11):116010.
94. Reinstein DZ, Archer TJ, Gobbe M. Stability of LASIK in corneas with topographic suspect keratoconus, with keratoconus excluded by epithelial thickness mapping. J Refract Surg. 2009;25(7):569–77.
95. Reinstein DZ, Archer TJ, Gobbe M. Stability of LASIK in corneas with topographic suspect keratoconus confirmed non-keratoconic by epithelial thickness mapping: 2-years follow-up. San Francisco: AAO; 2009.